EC COST B21
Physiological Modelling of MR Image Formation

MR imaging of kidney structure and function

(work in it's beginning)

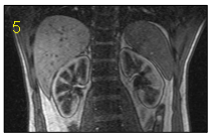

Arvid Lundervold MD, PhD

Department of Biomedicine
University of Bergen
NORWAY

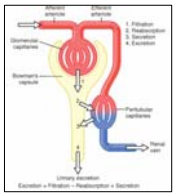

COST B21 WG 1 Meeting, Alghero, Sardinia, March 30th 2006

The future of nephrology

MR imaging of the kidneys
- structure & function

→ Data (parameter estimation)

"Computational Nephrology"
Modelling / Simulation

→ Computational MODEL

→ **Diagnosis** & **Prognosis**

Renal diseases in modern society

Incident Counts and Adjusted Rates of ESRD by Primary Diagnosis

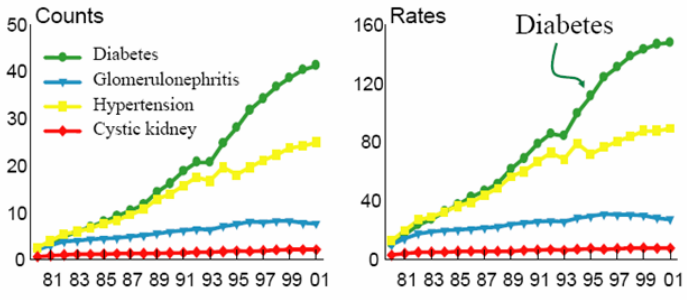

Incident ESRD patients; Medical Evidence form data; rates adjusted for age, gender, & race.

<u>In USA today:</u>

(pop. ~ 300 mill)

20 mill patients with chronic renal disease

450 000 **ESRD**

- 275 000 in dialysis

- 15 000 transpl./yr

80 000 dies from renal disease/yr

3 mill. new patients / yr. with renal disease !

ESRD = End stage renal disease (→ dialysis, transplantation)
GFR < 10% of normal

Arvid Lundervold, UIB

Renal diseases in modern society

(the effect of aging ...)

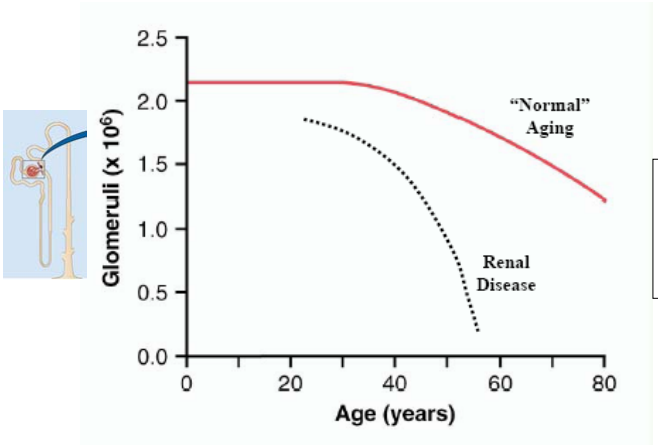

Symptoms of renal failure when number of nephrons is lower than 25% of normal, i.e. < 500 000 functional units

Arvid Lundervold, UIB

ELSEVIER

Seminars in ULTRASOUND CT and MRI

Magnetic Resonance Imaging of the Kidney

Nomdo S. Renken, MD, and Gabriel P. Krestin, MD, PhD

High tissue contrast, multiplanar image capabilities, and tissue characterization render MR into an ideal imaging modality for effective evaluation of a wide range of renal disorders.

It provides high details of anatomy and can suggest the composition of lesions. Improvements of MRI technology during the last years have made MRI increasingly attractive for body imaging. Fast imaging sequences and parallel imaging techniques have proved to be useful in minimizing artifacts from respiratory motion and magnetic susceptibility differences providing superior imaging quality.

Additionally, the use of renally eliminated paramagnetic contrast agents permits assessment of parenchymal perfusion and visualization of the excretion of the contrast medium providing information on renal function.

Semin Ultrasound CT MRI 26:153-161 © 2005 Elsevier Inc.

Arvid Lundervold, UIB

Renal cell carcinoma of the left kidney stage T3B with a large mass and tumor thrombus in the left renal vein and the inferior vena cava

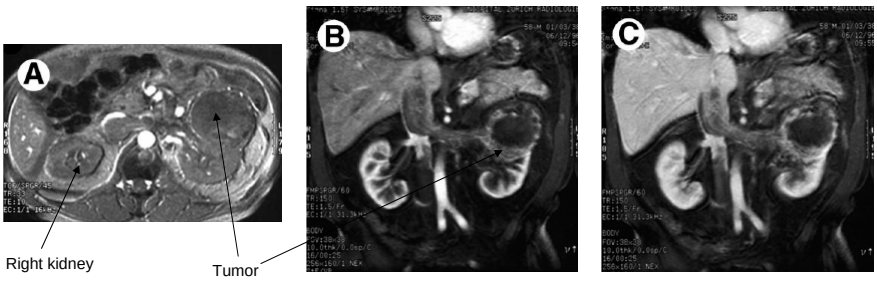

(A) Time of flight image demonstrating the mass within the left renal vein and inferior vena cava with partial flow surrounding the tumor thrombus.

(B) Early post contrast image.

(C) Delayed post contrast image with partial enhancement of the tumor thrombus on the delayed post contrast images.

Renkin & Krestin, 2005

Arvid Lundervold, UIB

Macroscopic and microscopic kidney architecture

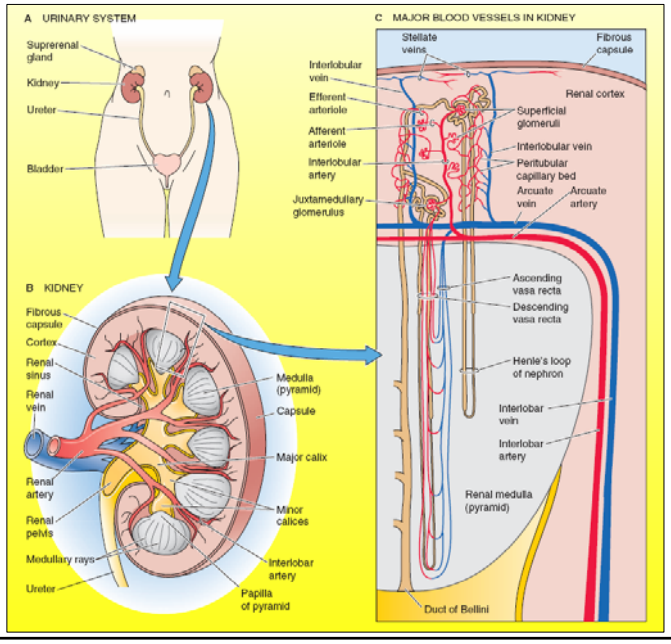

~10^6 nephrons

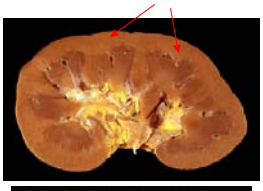

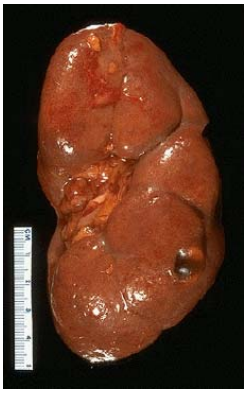

Arvid Lundervold, UIB

Renal microcirculation

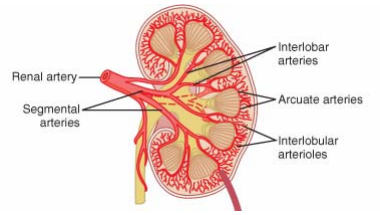

Diagram illustrating the principles of the renal microcirculation. The afferent arteriole, which is a branch of the interlobular artery, enters the glomerular capillary tuft at the vascular hilum. The emerging vessel, the efferent arteriole, normally divides into a complex system of capillaries, the peritubular capillary network, which surrounds the cortical tubules. The venous tributaries arising from the peritubular capillary network drain into small veins opening into the interlobular vein, which runs vertically alongside the interlobular artery and drains into the arcuate vein running alongside the arcuate artery at the corticomedullary junction. Close to the corticomedullary junction some of the efferent arterioles give rise to vertically running vessels, the vasa recta, which pass down into the medulla alongside the medullary duct and tubular systems. Some vasa recta arise as direct branches of the arcuate artery and drain directly into the arcuate vein.

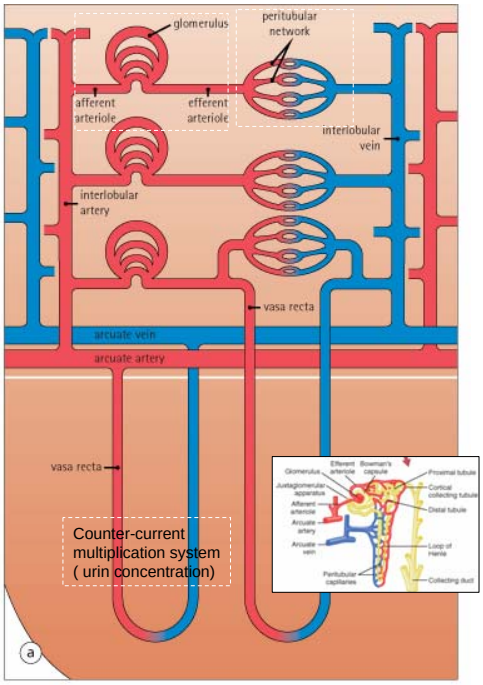

Arvid Lundervold, UIB

Measuring the renal transport – conservation of mass :

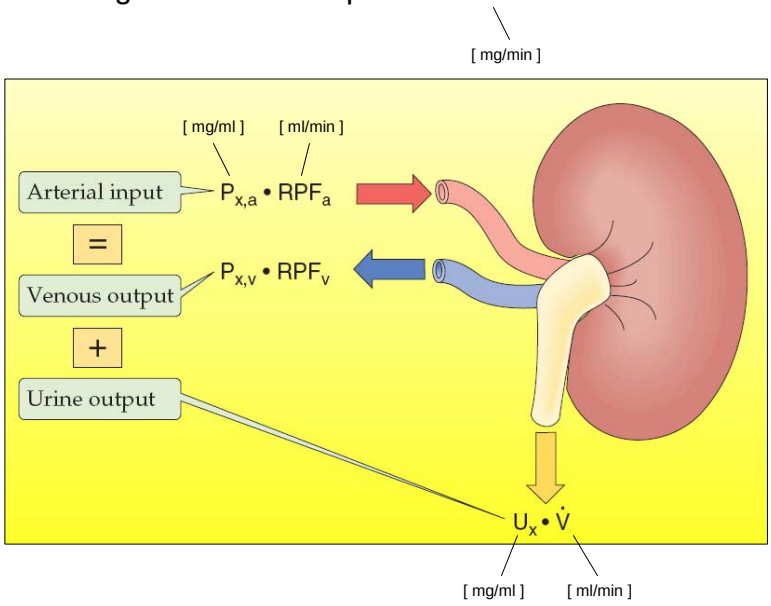

Arvid Lundervold, UIB

The functional anatomy of the glumerulus

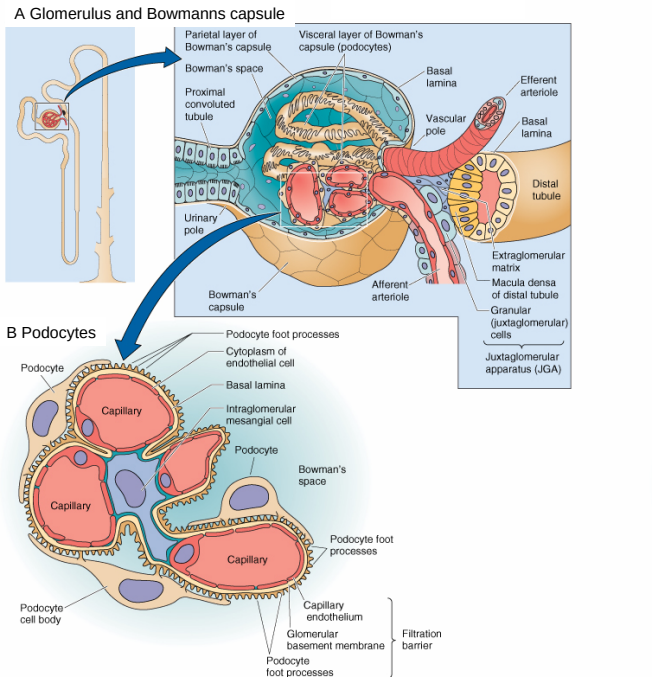

Arvid Lundervold, UIB

The glomerular filtration barrier ...

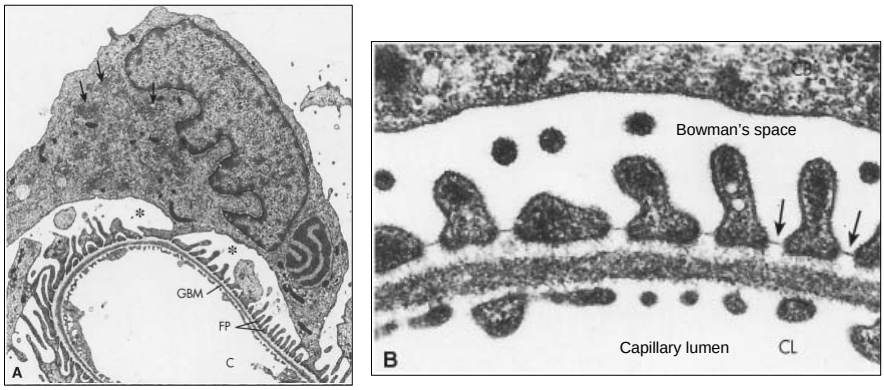

Electron micrograph of a podocyte surrounding a glomerular capillary. The cell body of the podocyte contains a large nucleus with three indentations. Cell processes of the podocyte form the interdigitating foot processes (FP). The arrows in the cytoplasm of the podocyte indicate the well-developed Golgi apparatus, and the asterisks indicate Bowman's space. C, capillary lumen; GBM, glomerular basement membrane. B, Electron micrograph of the filtration barrier of a glomerular capillary. The filtration barrier is composed of three layers: the endothelium, basement membrane, and foot processes of the podocytes. Note the diaphragm bridging the floor of the filtration slits (arrows). CB, cell body of a podocyte; CL, capillary lumen. (From Kriz W, Kaissling B. In Seldin DW, Giebisch G, eds: The kidney: physiology and pathophysiology, ed 2, New York, 1992, Raven Press.)

Arvid Lundervold, UIB

The glomerular filtration barrier ...

(seen from within a glomerular capillary)

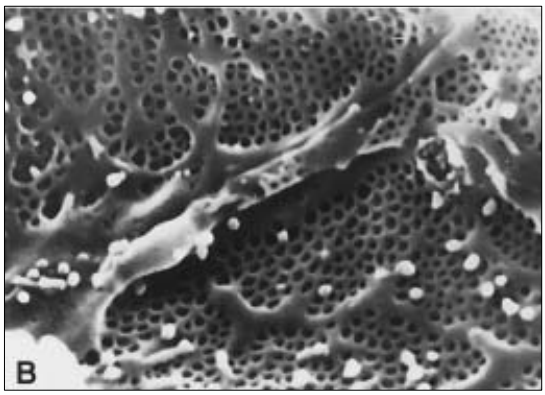

Scanning electron micrograph showing the outer surface of glomerular capillaries. This is the view that would be seen from Bowman's space. Processes (P) of podocytes run from the cell body (CB) toward the capillaries, where they ultimately split into foot processes. Interdigitation of the foot processes creates the filtration slits. B, Scanning electron micrograph of the inner surface (blood side) of a glomerular capillary. This view would be seen from the lumen of the capillary. The fenestrations of the endothelial cells are seen as small 700-Å holes. (From Kriz W, Kaissling B. In Seldin DW, Giebisch G, eds: The kidney: physiology and pathophysiology, ed 2, New York, 1992, Raven Press.)

Arvid Lundervold, UIB

Glomerular filtration rate (GFR) – a major functional parameter of the kidney

[ml/min]

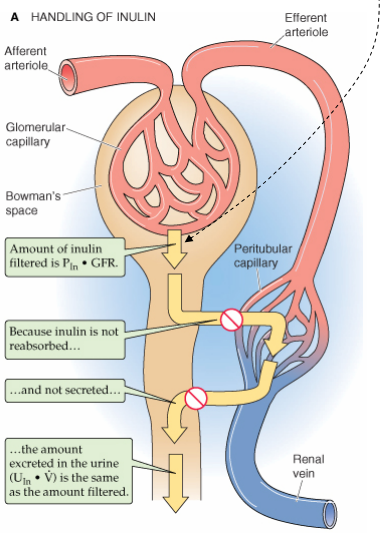

The Starling forces affecting ultrafiltration

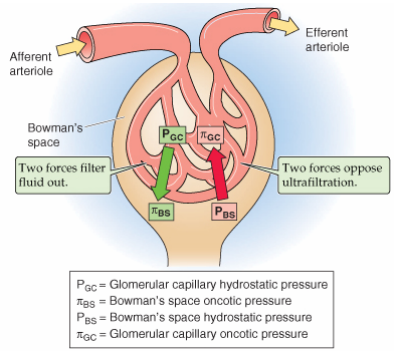

Arvid Lundervold, UIB

Structural MRI kidney data from Bergen

SEGMENTATION OF KIDNEYS FROM MR-IMAGES

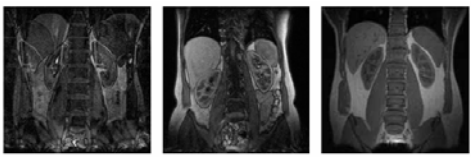

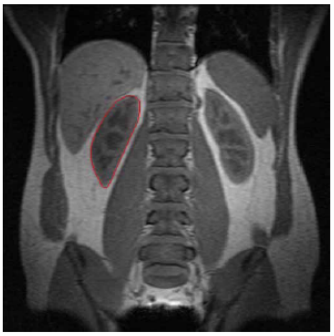

Eirik Roald Ree
Bergen 16. June 2005

The 3T MR machine at Haukeland University Hospital

Arvid Lundervold, UIB

Active Contours Without User Interaction

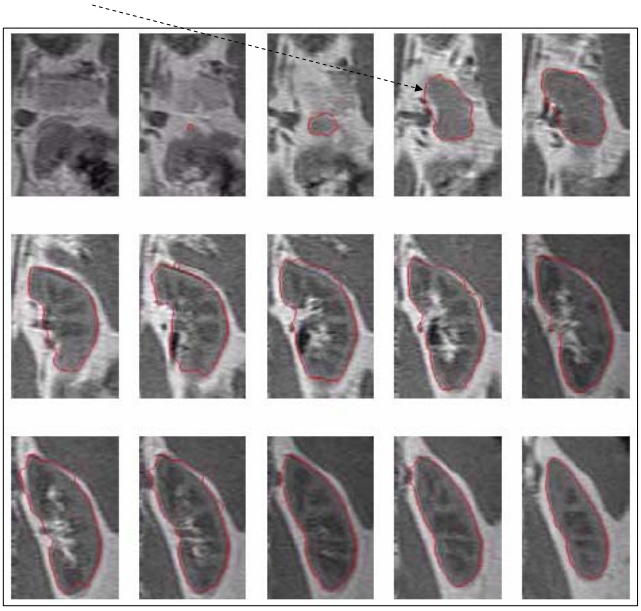

Eirik Ree, Diploma thesis, Bergen 2005

Arvid Lundervold, UIB

Estimation of renal volumes from MR images

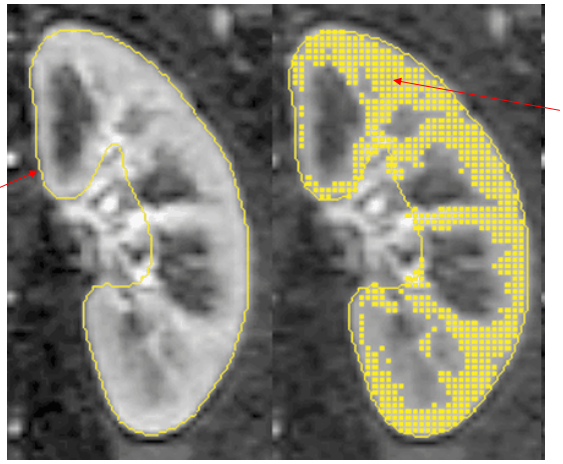

Figure 1. Measurement of total renal and renal cortex volumes on coronal 3D gadolinium-enhanced gradient-echo MR angiograms (4.3/1.3, 40° flip angle, 400-mm field of view, one signal acquired, 256 x 512 matrix, 2.6-mm section thickness) Left: Image shows the contour drawn around a kidney by the computer algorithm after exclusion of the renal hilum. Summation of all voxels within the contour yields the total renal volume. Right: After thresholding, the cortex volume can be measured by adding the enhancing voxels of the cortex. The small squares do not represent the actual pixel size.

Van den Dool et al. *Radiology* 2005

Arvid Lundervold, UIB

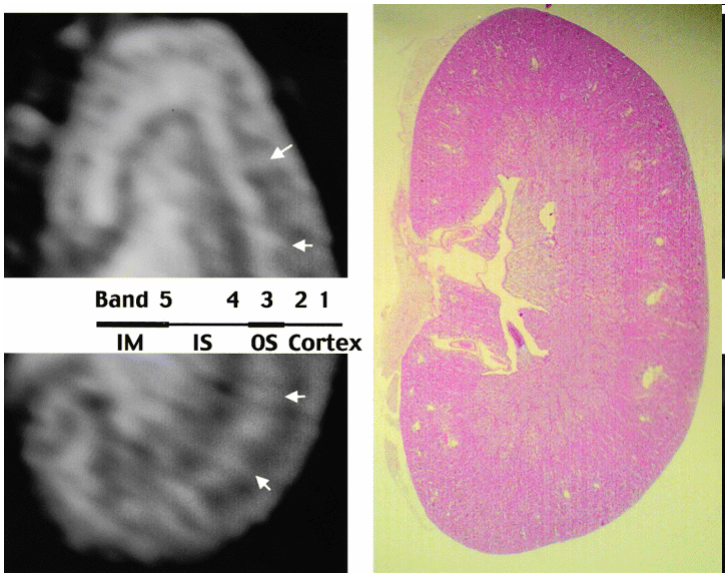

Fig. 2. Comparison of micro-MR image (left) and H&E stained section of kidney (right). The cortex, outer stripe (OS) and inner stripe (IS) of the outer medulla, and urinary space/inner medulla (IM) are labeled. Radial spikes (medullary rays) that extend from the outer strip into the superficial cortex are indicated by white arrows.

Kobayashi et al. Kidney International 61 (6), 1980-1985.

Arvid Lundervold, UIB

Dynamic Three-dimensional MR Renography for the Measurement of Single Kidney Function (Vera Lee et al.)

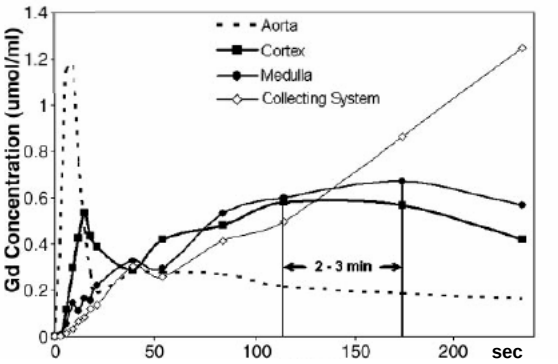

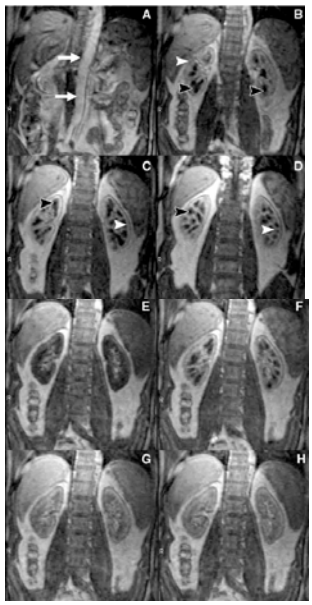

Results of 3D MR renography of the right kidney in a 59-year-old woman with hypertension (GFR = 31 mL/min on the basis of 99mTc-DTPA clearance and gamma camera split renal function). Measured 3D MR renographic signal intensities were converted to gadolinium *(Gd)* concentrations. Renal cortical, medullary, and collecting system enhancement curves are plotted along with measurements for the aorta. This case shows typical patterns of enhancement in each intrarenal compartment and illustrates the measurements during 2–3 minutes after injection that were used to compute split renal function and single kidney MR GFR index. (Lee et al, *Radiology* 2003)

Arvid Lundervold, UIB

Dynamic MRI kidney data from Bergen

Kidney function / Image registration project (with A. Santos & R. Sance, Madrid)

Abdominal (kidney) dynamic contrast enhanced 3D FLASH acquisitions (healthy volunteer)
Siemens Symphony 1.5 T (TR = 3.3 / TE = 1.79 / FlipAngle = 9deg)

Series desc. T1_fl3d_COR_bh_pat2_2_5SEK e.g. from >> info = dicominfo('27979190')

DICOM images are converted to MATLAB (v. 7.0) matrix VTS (256 x 256 x 20 x 20), stored in 'bergen_capio_20050419_kidney_volume_timeseries.mat'

Dimension 0	256
Dimension 1	256
Dimension 2	20 (slices)
Dimension 3	20 (time frames)
Type	Short
Min	0.0
Max	143.0
Pixel resolution 0	1.48 Millimeters
Pixel resolution 1	1.48 Millimeters
Pixel resolution 2	3.0 Millimeters (slice thickness)

```
>> load bergen_capio_20050419_kidney_volume_timeseries.mat
>> mx = max(VTS(:))
>> X10 = reshape(VTS(:,:,10,:)/mx, 256, 256, 1, 20);
>> montage(X10);
```

bergen_capio_20050419_info.doc

Arvid Lundervold, UIB

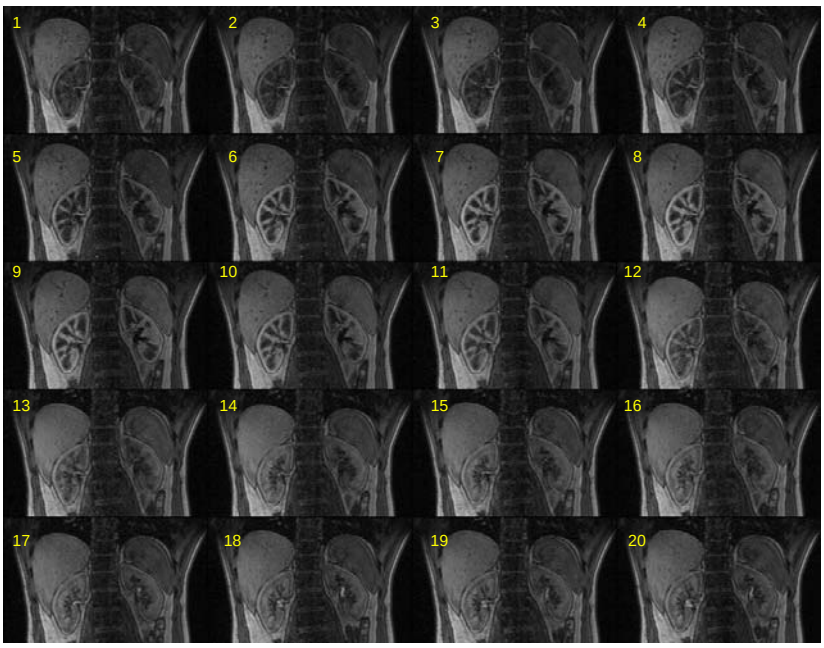

bergen_capio_20050419_kidney_volume_timeseries.mat 20 slices, 20 time frames, voxel-size: 1.48 x 1.48 x 3 mm^3

get_timing_information_capio_20050419_kidney_vts_20060329.m

Arvid Lundervold, UIB

Dynamic imaging of the kidneys - and the need for motion correction

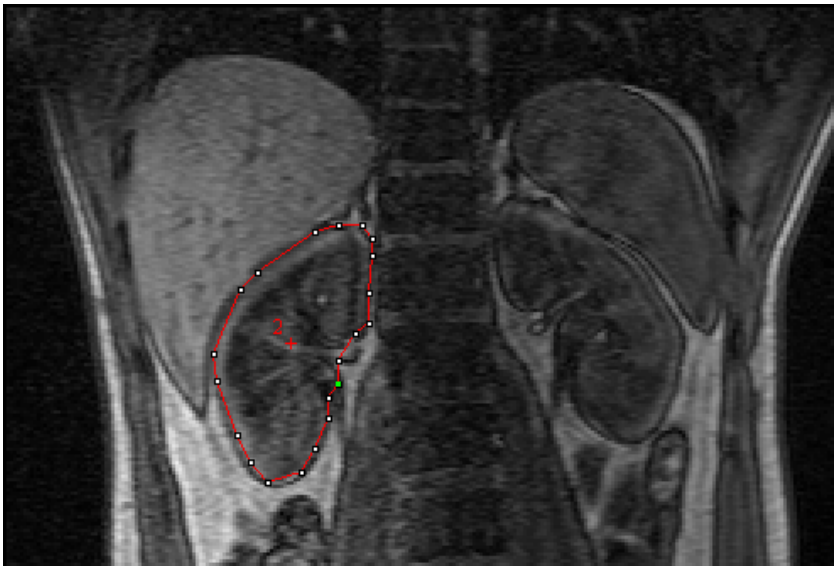

Timeline:

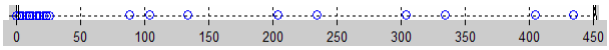

Left kidney: slice 10, frame 20

bergen_capio_20050419_kidney_volume_timeseries.mat 20 slices, 20 time frames, voxel-size: 1.48 x 1.48 x 3 mm^3 Initially: 2.5 s/frame

Arvid Lundervold, UIB

José M. F. Moura, "**MRI Techniques for Noninvasive Monitoring of Transplanted Organs**"

(Electrical and Computer Engineering, Carnegie Mellon University)

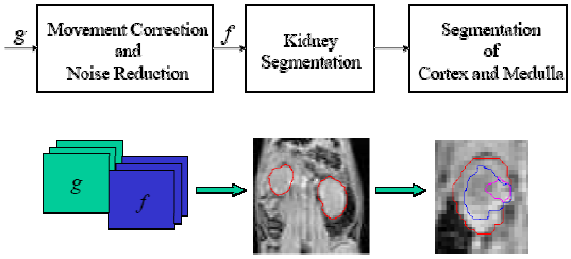

Given the observed image sequence $g(i, j, t)$, find the image sequence $f(i, j, t)$ that minimizes

$$E = \underbrace{\|g - Hf\|^2}_{\text{Motion correction}} + \underbrace{\alpha\|\nabla_t f\|^2_W + \beta\|\nabla_{tt} f\|^2_W}_{\text{Weighted temporal smoothness constraints}}$$

Assume the variance of the background noise is σ^2

$$w(i, j, t) = \exp(1/2)\exp\left(-\frac{p(i, j, t)}{2\sigma^2}\right)$$ Selectively Smooth

$$p(i, j, t) = \frac{1}{2m+1}\sum_{k=-m}^{m}(g(i, j, t+k) - \bar{g}(i, j, t))^2 \qquad \bar{g}(i, j, t) = \frac{1}{2m+1}\sum_{k=-m}^{m} g(i, j, t+k)$$

To be implemented by Andrea Anderlik, UiB

Arvid Lundervold, UIB

Image registration for quantitative analysis of kidney function using MRI

Rosario Sance[1], María J. Ledesma-Carbayo[1], Arvid Lundervold[2] and Andrés Santos[1]

[1]Universidad Politécnica de Madrid, Madrid, Spain
[2]University of Bergen, Bergen, Norway

STSM Bergen, May 2006

(Submitted to WIO Toledo, 2006)

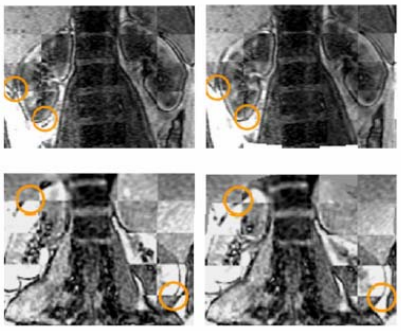

Figure 2: Registration results. Composite images before (*left*) and after (*right*) alignment. Slices corresponding to a 1.5 T (*upper*) and a 3.0 T (*lower*) DCE-MRI series.

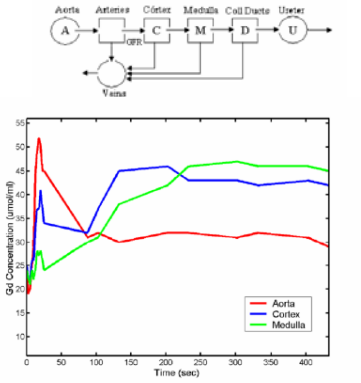

Figure 3: Compartmental Gd concentration versus time.

Arvid Lundervold, UIB

Choyke PL, Kobayashi H. Abdom Imaging. 2005 Nov 10;

Functional magnetic resonance imaging of the kidney using macromolecular contrast agents

Background Functional magnetic resonance (MR) imaging of the kidney relies on low-molecular-weight contrast agents. *These agents are glomerular filtration markers and are neither secreted nor reabsorbed by the tubules but are filtered at the glomerulus.* Low-molecular-weight contrast agents provide limited functional information. A new generation of macromolecular magnetic contrast agents is under development for MR angiography. These agents may provide additional renal functional information not provided by low-molecular-weight agents.

Methods We review the use of macromolecular contrast agents such as gadolinium-bound albumin (Gd-albumin), gadolinium-bound dendrimer (Gd-dendrimer), and ultrasmall particles of iron oxide (USPIO) in specific renal parenchymal diseases. These data are largely derived from animal studies because many of these agents have not been extensively deployed in human populations.

Results Different specific uses have been documented for macromolecular contrast agents. Gd-albumin appears to detect the source of proteinuria and localize the site of recurrent proteinuria after transplantation. Gd-dendrimer uptake reflects damage to the proximal straight tubule in the outer medulla. USPIO agents demonstrate sites of inflammatory changes within the kidney.

Conclusions Although not yet in widespread clinical use, macromolecular MR contrast agents may play a role in the evaluation of functional diseases of the kidneys.

Arvid Lundervold, UIB

Dynamic imaging in experimental kidney disease of different functional severity

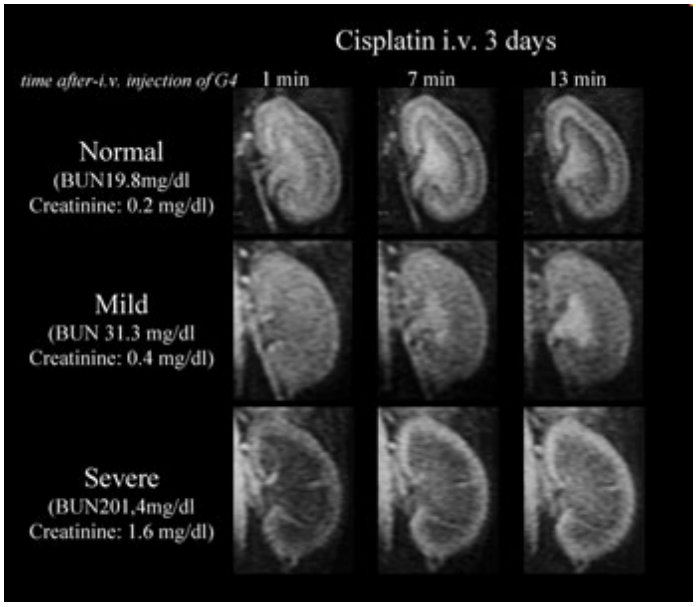

Comparison of normal, mild, and severe cisplatin nephrotoxicities in an animal model.

The normal kidney demonstrates the characteristic outer medullary stripe, which is better seen by 13 min. Even in mild nephrotoxicity, this stripe is no longer seen, although excretion into the renal pelvis can be perceived.

In severe nephrotoxicity, only the cortex opacifies with contrast medium due to acute tubular necrosis.

BUN = blood urea nitrogen

Choyke PL, Kobayashi H. Abdom Imaging. 2005 Nov 10;

Arvid Lundervold, UIB

Comparison of different causes of renal failure and their effects on the appearance of the kidney

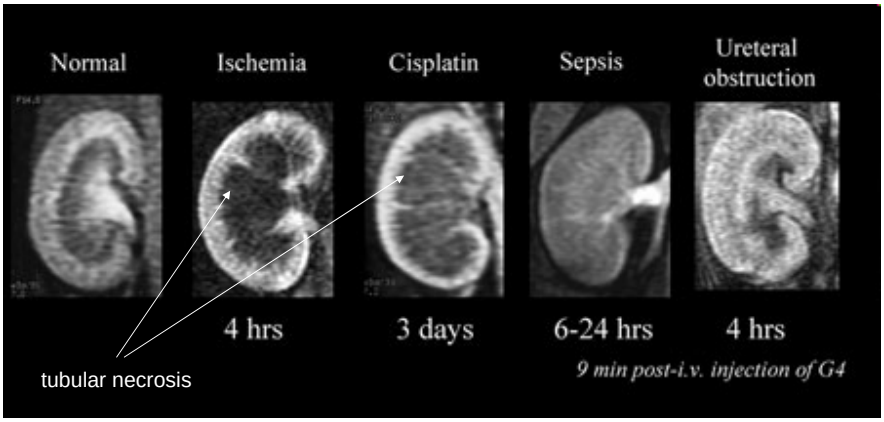

Left to right An ischemic kidney and severe cisplatin toxicity demonstrate similar acute tubular necrotic features. Sepsis at 6 to 24 h demonstrates loss of the stripe but continued opacification of the renal medulla. There is also loss of the stripe in renal obstruction in addition to delayed excretion.

Choyke PL, Kobayashi H. Abdom Imaging. 2005 Nov 10;

Arvid Lundervold, UIB

Magnetic Resonance in Medicine 53:545–552 (2005)

Sodium Magnetic Resonance Imaging of Diuresis: Spatial and Kinetic Response

Nimrod Maril,[1] Raanan Margalit,[1] Joel Mispelter,[2] and Hadassa Degani[1]*

Renal function is highly correlated with the sodium concentration gradient along the corticomedullary axis. The application of 3D high-resolution sodium magnetic resonance imaging (MRI) provided a means to quantify in vivo the spatial and temporal changes in renal tissue sodium concentration under normal and diuretic conditions.
A detailed, pixel-by-pixel analysis of the intact rat kidney sodium MR images yielded a quantitative measure of the corticomedullary sodium gradient before and at early and later times after the administration of two distinct diuretic agents, furosemide and mannitol. Furosemide, a loop diuretic, induced a fivefold reduction in the cortical-outer medullary sodium gradient, whereas mannitol, an osmotic diuretic, did not affect this gradient. Both diuretics induced a 50% decrease in the sodium concentration of the inner medulla; however, mannitol exerted its effect twice as fast as furosemide with a 2.5-min exponential decay constant. These specific changes were attributed to the different mechanism of action and site of activity of each diuretic agent. Thus, high-resolution ^{23}Na MRI offers a unique, noninvasive tool for functional imaging of the kidney physiology.

Arvid Lundervold, UIB

Sodium Magnetic Resonance Imaging of Diuresis: Spatial and Kinetic Response

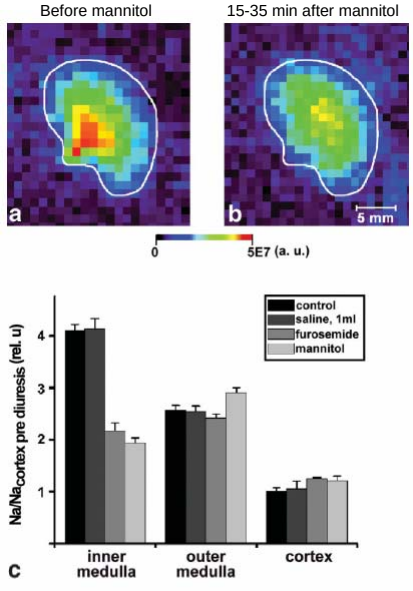

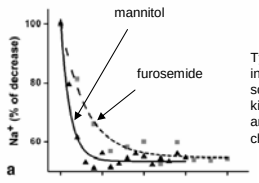

Typical time courses of diuresis induced changes in regional sodium levels of an intact rat kidney. (**a**) Furosemide- (square) and mannitol (triangle)-induced changes in the inner medulla.

FIG. 4. Diuretic-induced changes in renal sodium distribution. (**a**) and (**b**) Typical coronal ^{23}Na MR images of a kidney recorded before and 15–35 min (steady state) after a bolus injection of mannitol (0.1 N, 1 mL), respectively. (**c**) Sodium relative level in the cortex and outer and inner medulla of control kidneys (n = 20), kidneys treated with saline (n = 3), kidneys treated with furosemide (n = 7), and kidneys treated with mannitol (n = 7). The images in A and B were recorded using a 3D gradient echo sequence with TE/TR of 1.7/60 ms, spatial resolution of 0.94 × 0.94 × 5 mm^3, and 20 min scanning time. The sodium level was measured using an ROI-based analysis. Sodium relative level in control kidneys was determined from the signal intensity in each region relative to that in the cortex. Sodium relative level in the treated kidneys was determined from the sodium signal intensity in each region posttreatment relative to the intensity in the cortex of the same kidneys pretreatment.

Maril et al. Magn Reson Med 2005;53:545–552

Arvid Lundervold, UIB

Permeability mapping (tumor)

[parameter estimation in pharmacokinetic models]

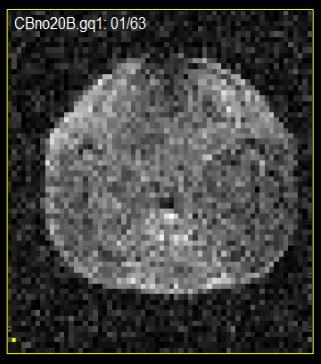

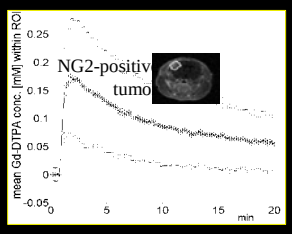

Two compartment model:

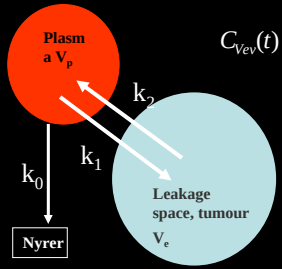

$$C_{Vev}(t) = v_p C_p(t) + v_e C_e(t)$$

$$\frac{dC_e}{dt} = k_1 C_p - k_2 C_e$$

$$\frac{dC_p}{dt} = k_2 C_e - k_1 C_p - k_0 C_p$$

Brekke et al., Neuroimage 2006

Multiparametric and repeated MRI measurements

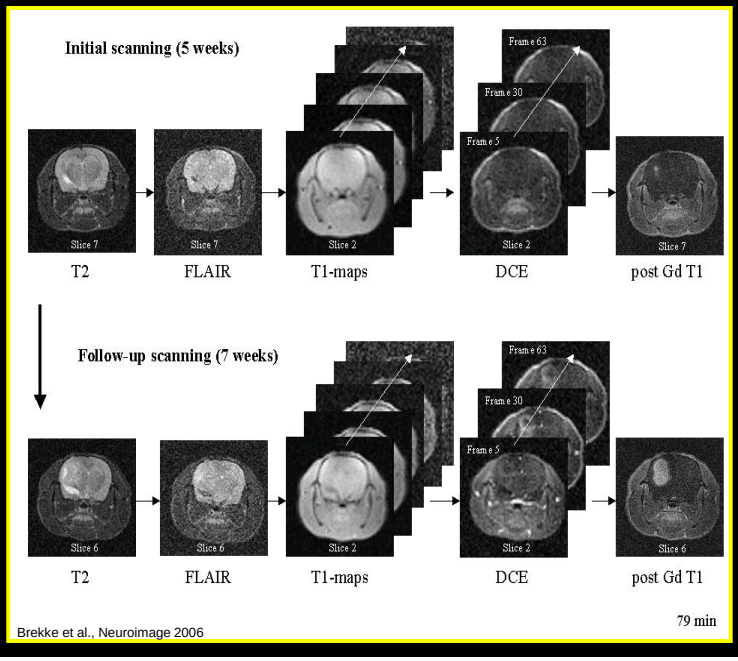

Brekke et al., Neuroimage 2006

Multispectral imaging

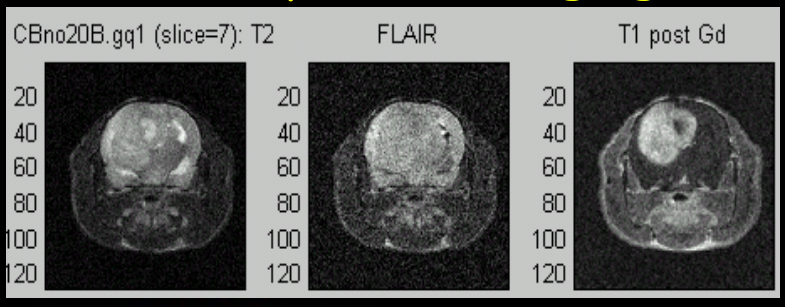

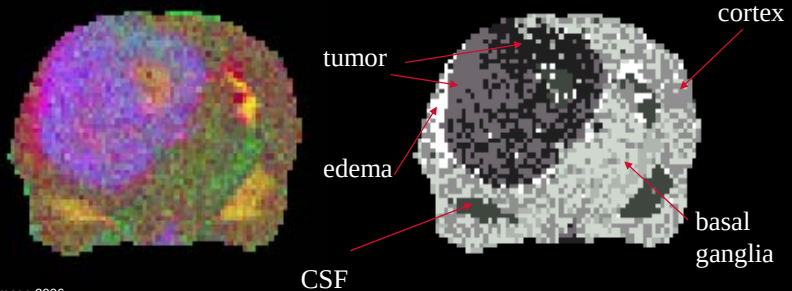

Brekke et al., Neuroimage 2006

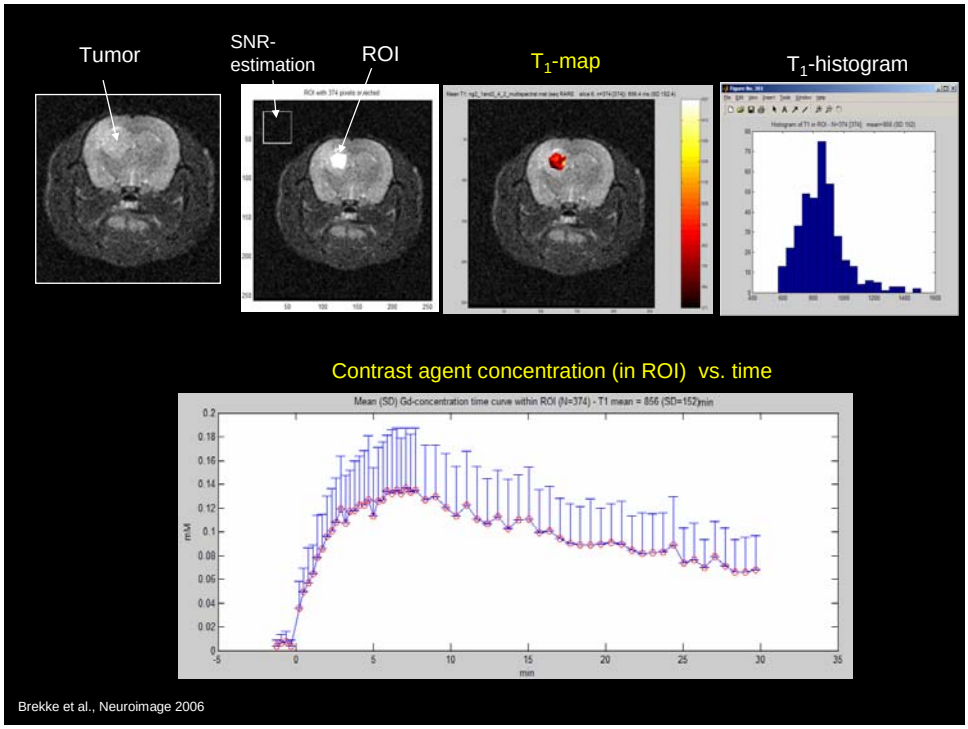
Tumor
SNR-estimation
ROI
T_1-map
T_1-histogram
Contrast agent concentration (in ROI) vs. time
Mean (SD) Gd-concentration time curve within ROI (N=374) - T1 mean = 856 (SD=152)min
mM
min
Brekke et al., Neuroimage 2006

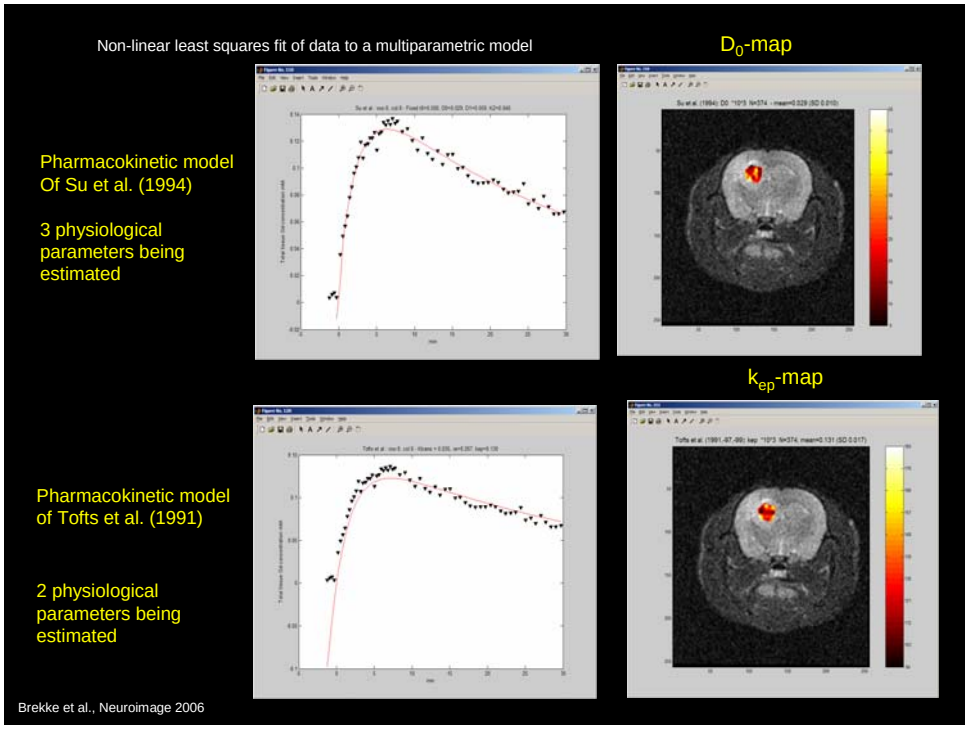
Non-linear least squares fit of data to a multiparametric model
D_0-map
Pharmacokinetic model Of Su et al. (1994)
3 physiological parameters being estimated
k_{ep}-map
Pharmacokinetic model of Tofts et al. (1991)
2 physiological parameters being estimated
Brekke et al., Neuroimage 2006

”Computational Nephrology”

Modeling / Simulation

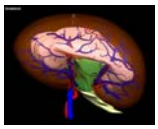

The future of nephrology

MR imaging of the kidneys
- structure & function

→ Data (parameter estimation)

”Computational Nephrology”
Modelling / Simulation

→ Computational MODEL

→ **Diagnosis** & **Prognosis**

Physiomics

= *the emerging quantitative physiology that is needed to integrate molecular and genetic information through physiological function*

Arvid Lundervold, UIB

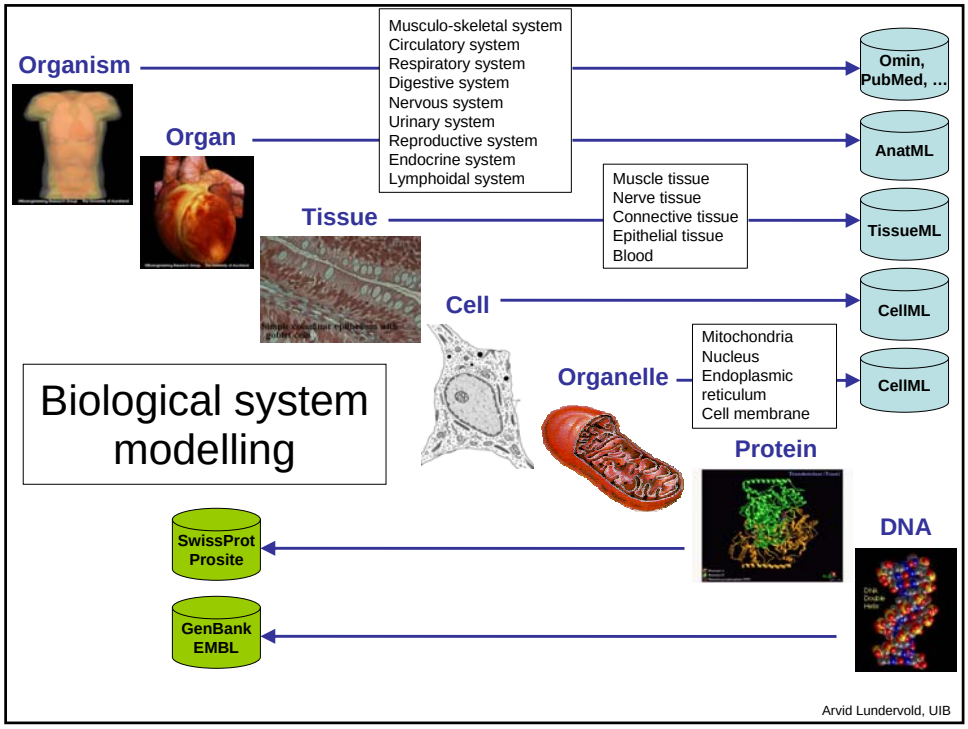

Outputs of computational modelling

e.g. the Physiome project: www.physiome.org

- *In-silico* disease models
- Patient-specific models
- Rational drug design

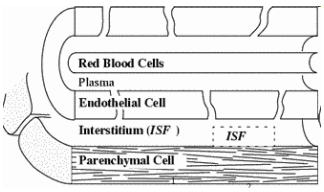

- Web-based physiological collaboratories
- Better educational tools

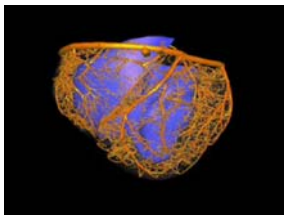

Arvid Lundervold, UIB

Estimation of Extraction Fraction (EF) and Glomerular Filtration Rate (GFR) Using MRI: Considerations Derived From a New Gd-Chelate Biodistribution Model Simulation

Michael H. Buonocore* and Richard W. Katzberg

Previous reports have described the use of magnetic resonance imaging (MRI) to estimate single-kidney extraction fraction (EF) and glomerular filtration rate (GFR), by measuring the concentration difference of intravenously injected Gd-chelate ([Gd]) in the renal artery and renal vein from measurements of blood T1.

Problematic is the fact that [Gd] measurements in the renal artery are often inaccurate due to the small size, tortuousness and motion of the vessel. Consequently, the [Gd] in the inferior vena cava (IVC) below the renal vein ostia (i.e., the infrarenal IVC) has been used instead of the renal artery [Gd], based on the assumption that the [Gd] in the infrarenal IVC is the same as it is in the renal artery. However, this assumption has neither been theoretically nor experimentally investigated.

Herein, we describe new difference and differential equation pharmacological models that can predict the biodistribution of Gd-chelate throughout the extracellular space. Assuming known average normal blood flows and GFR, our models predict that the infrarenal IVC [Gd] is 3.2% to 4.7% greater than the renal artery [Gd], and that the EF estimate using this IVC measurement is overestimated by 14.2%-20.0%. To support these predictions, algebraic equations are derived which show that the infrarenal IVC must develop a relatively high [Gd] in order to satisfy Gd flux constraints within the vascular system. These results suggest that the infrarenal IVC [Gd] is not a valid substitute for the renal artery [Gd].

Arvid Lundervold, UIB

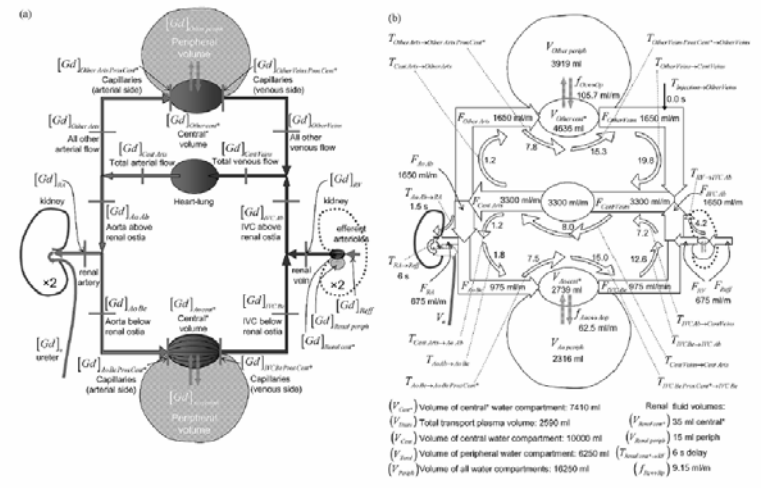

Fig. 1. Model of the vascular geometry and water compartments. The dotted kidney with internal vasculature and water compartments on the right represents the same kidney as on the left. The drawings represents both kidneys, along with associated ureters, renal arteries and veins, and shows blood flows, compartment volumes, and exchange rates for both kidneys. (a) This figure identifies the principal circuits of blood flow and compartments of Gd exchange. Mathematical symbols used for representing the Gd concentrations ([Gd]) are shown. Thick lines cutting through the vessels identify locations where [Gd] is tracked in the simulation. (b) This figure shows the model with numerical values for compartment volumes, exchange rates, plasma flows, and transit times representative of a healthy resting 70-kg adult male used in the simulation. Mathematical symbols used for representing the plasma flow (F) and the transit times (T) are also shown. Plasma flows are given in units of ml/min (ml/m) within the straight or right-angle open arrows. Exchange rates are given in units of ml/min (ml/m) adjacent to paired arrows. Transit times are given in units of seconds (not labeled) adjacent to thin curved open arrows. Central and peripheral volumes are given in units of milliliters. Renal flows, renal water volumes and GFR reflect the combined hemodynamics of both kidneys.

Arvid Lundervold, UIB

The Kidney Simulation Project

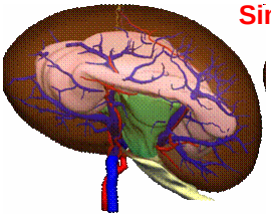

The aim of the Kidney Simulation Project is to use advanced data analysis and modelling techniques to integrate functional and structural biological data at gene, cell, tissue and organ levels into a computer based model of the mammalian kidney. The project is a collaboration between the departments of Information Systems and Physiology at Melbourne Uni, and the Bioengineering Institute at Auckland Uni.

There are three aspects to the project:

1. A **mathematical modelling** approach that aims to reconstruct 'normal' kidney function by integrating quantitative cell models into functional segments of the nephron (the functional unit of the kidney).

2. A **conceptual/qualitative modelling** approach that uses manual reviewing and natural language processing to analyse scientific literature, in order to construct high level models of kidney physiology and renal dysfunction.

The idea is that these two approaches, one top-down and the other bottom-up, are complementary and will eventually allow us to integrate physiology with cell function.

3. Using **visual anatomy** of the kidney as an interface for knowledge representation.

http://www.dis.unimelb.edu.au/staff/andrewl/KidneySim.htm

Arvid Lundervold, UIB

Structural and functional representation

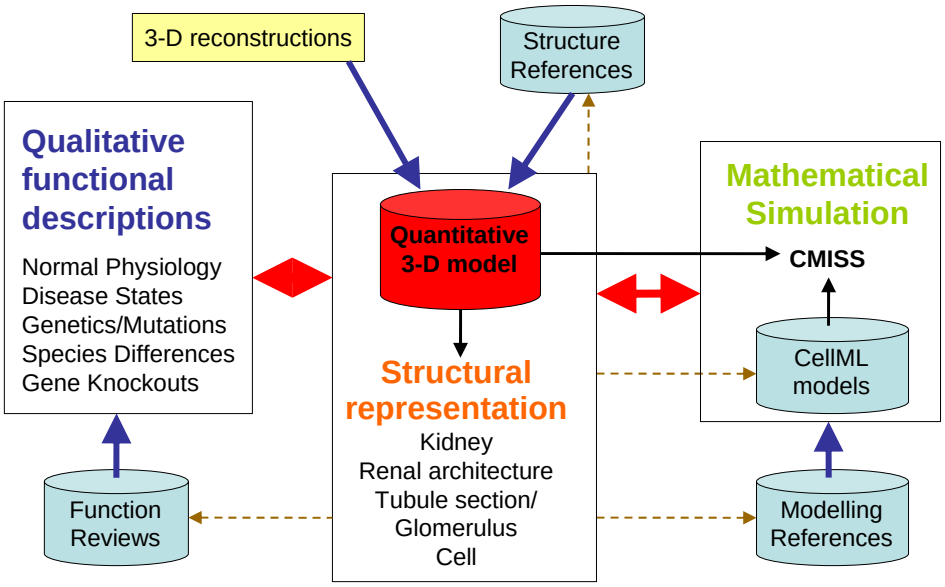

http://www.dis.unimelb.edu.au/staff/andrewl/KidneySim.htm

Arvid Lundervold, UIB

Challenges i MRI of the kidney:

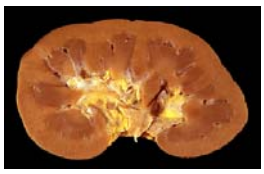

- Measurment techniques (spatial and temporal resolution)
- Design of new contrast agents – molecular imaging
- Image segmentation & morphometry (global, regional)
- Image registration (deformation and signal intensity variations)
- Voxel-based tracer kinetics
- Image based physiological modelling
- Increasingly important clinical applications

Arvid Lundervold, UIB

Thanks !

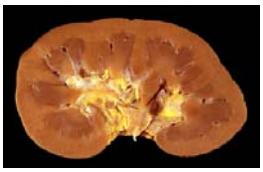

Arvid Lundervold, UIB